11th International Symposium on Turbulence and Shear Flow Phenomena (TSFP11)
Southampton, UK, July 30 to August 2, 2019

ASSESSMENT OF RANS TURBULENCE MODEL PERFORMANCE IN TIGHT LATTICE LWR FUEL SUBCHANNELS

Dean Wilson
School of MACE
The University of Manchester
Oxford Road, Manchester, M13 9PL
dean.wilson@manchester.ac.uk

Hector Iacovides
School of MACE
The University of Manchester
Oxford Road, Manchester, M13 9PL
h.iacovides@manchester.ac.uk

Tim Craft
School of MACE
The University of Manchester
Oxford Road, Manchester, M13 9PL
tim.craft@manchester.ac.uk

ABSTRACT

Reynolds-averaged Navier-Stokes simulations have been performed of the turbulent flow ($Re = 48000$) through a tight lattice ($P/D = 1.194$) subchannel typical of those found in nuclear thermal-hydraulic applications. A wide range of turbulence models (linear eddy-viscosity, non-linear eddy-viscosity and stress-transport) and the use of different near-wall treatments (low-*Re*, standard and analytical wall-functions) have been considered.

The results demonstrate both the failure of the standard wall function approach in reproducing flows with significant near-wall convection and pressure-gradient effects, and the limitations of using linear eddy-viscosity approaches in flows with anisotropic effects. Although models utilizing low-*Re* near-wall approaches demonstrated superior overall performance, the analytical wall-function tested offers improvements over the standard 'log-law' based formulation.

INTRODUCTION

Rod bundle type geometries, where a coolant flows axially between a series of cylindrical tubes arranged in a triangular or square pitch pattern, are frequently encountered in nuclear applications. They typically form the main fluid flow passages within the core of light water type nuclear reactors, creating a series of interconnected subchannels with generally non-circular cross-sections.

It is well known that any wall-bounded turbulent flow of non-circular cross section will display mean fluid motion in a plane perpendicular to the main axial flow (Prandtl's 'secondary motion of the second kind'), owing to the anisotropic distribution of the cross-stream normal stresses. Whilst the magnitude of these motions is typically only 1-2 % of the mean axial flow, they do modify the axial velocity distribution within the cross-section and can thus affect thermal-hydraulic performance.

An experimental study by Hooper (1980) looked at the turbulent fully developed flow ($Re = 48000$) of air through a 2x3 square pitched rod bundle (i.e. two adjacent subchannel sections). Whilst providing detailed measurements of the mean flow and turbulent stresses at two different pitch to diameter ratios, Hooper could not accurately detect the presence of secondary flow. Horváth & Dressel (2012) conducted Reynolds-Averaged Navier-Stokes (RANS) simulations on a more general version of this geometry (single subchannel with lateral periodicity), applying both eddy-viscosity and stress-transport turbulence models with standard wall functions. Results demonstrated generally good agreement, with only the stress-transport type models being capable of reproducing the correct stress anisotropy (and hence secondary motion) as would be expected.

Current numerical modelling practice within the nuclear industry favours the use of thermal-hydraulic 'system codes' which use a number of limiting simplifications to provide a very coarse (typically 1D) numerical model of the entire reactor system. Whilst well validated for some nuclear specific test cases, the low fidelity of the results limits the depth of the analysis that can be performed and thus they cannot be expected to reproduce the kinds of flow details discussed above. Since CFD codes in general, and RANS turbulence models in particular, have now reached a degree of maturity, it is relevant to explore their potential for routine use in the computation of nuclear-relevant flows.

This study aims to demonstrate the potential of current state-of-the-art RANS turbulence models in modelling nuclear relevant subchannel type flows by reproducing the experimental results of Hooper (1980) using their exact geometric configuration, a wider range of more advanced turbulence models and different near-wall treatments. Detailed explorations of these flows will also help contribute towards the overall continued assessment and development of turbulence models within the RANS framework.

CASE SET-UP

The full wall-bounded twin subchannel geometry of Hooper is considered, consisting of 6 circular rods arranged in a 2x3 square array as shown by the schematic cross-section in Figure 1. All the gaps between the rods except for the two central rods were blanked in the experimen-

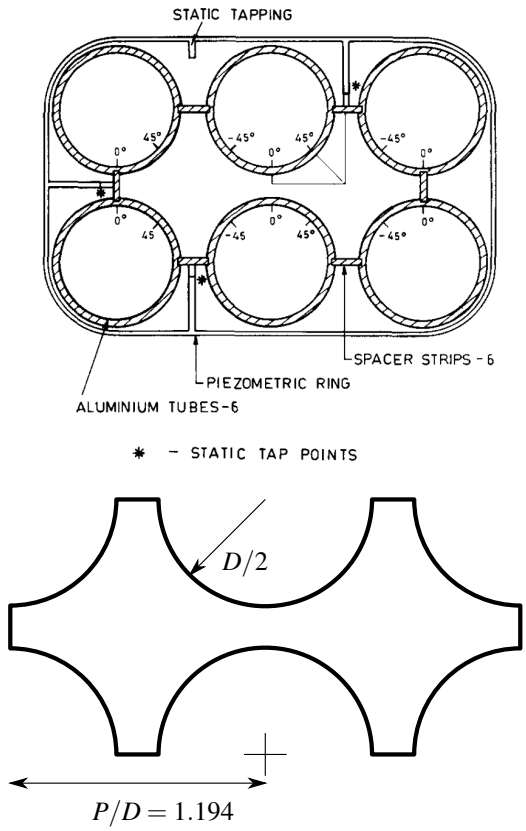

Figure 1. Cross-section of the experimental flow set-up used by Hooper (1980) (top) and geometry used for present simulations (bottom).

tal test-section, effectively creating two sub-channels interconnected by the remaining centre gap. The P/D ratio is chosen to be the larger of the two considered by Hooper, $P/D = 1.194$, since this is closer to the ratio typically encountered in modern LWR fuel assemblies ($P/D = 1.38$). As Hooper reported the flow to be fully developed, the axial length of the domain was reduced to just one cell with axial periodicity applied. An imposed pressure gradient was applied to drive the flow such that the Reynolds number, based on the bulk axial velocity and hydraulic diameter, was $Re = 48000$.

Turbulence Models

Table 1 details the turbulence models used within this work and these are chosen to provide representation across the three main classes of RANS model available; linear eddy-viscosity (LEVM), non-linear eddy-viscosity (NLEVM) and stress-transport (RSM). Models are additionally split according to their approach to the near-wall region, with both low-*Re* and several high-*Re* methodologies investigated (discussed in more detail below). Both high (`HR`) and low-*Re* (`LR`) forms of the 'standard' $k-\varepsilon$ two-equation model have been tested, along with the $k-\omega$ SST model (`FM`) of Menter (1994), which is a hybrid model that essentially blends a $k-\varepsilon$ type model in the far-field with a $k-\omega$ model near the wall through the use of a blending function. The Gibson & Launder (1978) RSM (`GL`), which adds a wall-reflection term to the 'isotropization' of production based model of Launder *et al.* (1975), and the Craft & Launder (1992) RSM (`CL`), which modified this wall-reflection term to more accurately account for flows with large wall-normal straining, have also been tested. The `KS` model extends the $k-\varepsilon$ model with the inclusion of cubic terms in the stress-strain relationship and has demonstrated good performance in flows affected by curvature and impingement (Craft *et al.*, 1996). Finally, the low-*Re* RSM of Jakirlić & Hanjalić (1995) (`HJ`), which aims to extend the applicability of the `GL` RSM closure to flows with significant low-*Re* and wall proximity effects (partly by expressing the coefficients in the $\overline{u_i u_j}$ equation as functions of the turbulent Reynolds number and invariants of the stress and dissipation rate tensors), has also been tested. This has demonstrated superiority to eddy-viscosity type models over a range of non-equilibrium Hanjalić *et al.* (1997) and swirling flows Jakirlic *et al.* (2002).

Table 1. Turbulence models and wall treatments used within this work, where RSM is Reynolds Stress Model and NL is Non-Linear.

Code	Type	Reference
High-Re - Wall function		
`HR`	$k-\varepsilon$	Launder & Spalding (1974)
`GL`	RSM	Gibson & Launder (1978)
`CL`	RSM	Craft & Launder (1992)
Low-Re		
`LS`	$k-\varepsilon$	Launder & Sharma (1974)
`FM`	$k-\omega$ SST	Menter (1994)
`KS`	NL $k-\varepsilon$	Craft *et al.* (1996)
`HJ`	RSM	Jakirlić & Hanjalić (1995)

Near-wall Modelling

In addition to the low-*Re* turbulence models used in this work, which all include additional damping terms to ensure validity in the near-wall sublayer, two wall-function approaches have been considered. The first, generally referred to as the standard wall-function (SWF), is based on the well-known *law of the wall* and uses the assumption of local equilibrium (amongst others) in the near-wall turbulence to formulate an expression for the velocity as a function of the distance from the wall. Despite enjoying substantive use over the past five or six decades, many of the underlying assumptions break down in even mildly complex flows; those involving impingement, rotation, separation or buoyancy for example. Their widespread use, however, means it is relevant to continue to assess their performance, even if it only serves to continue to highlight their weaknesses.

The second approach aims to correct many of the deficiencies in the SWF approach whilst retaining its overall framework and essence. Work conducted at UMIST during the early 2000's (Gerasimov, 2004; Craft *et al.*, 2002) led to the development of the so-called 'analytical wall function' (AWF). Instead of assuming local equilibrium, the approach accounts for pressure gradients, convection effects, and other force-fields such as buoyancy by solving simplified forms of the near-wall momentum and temperature

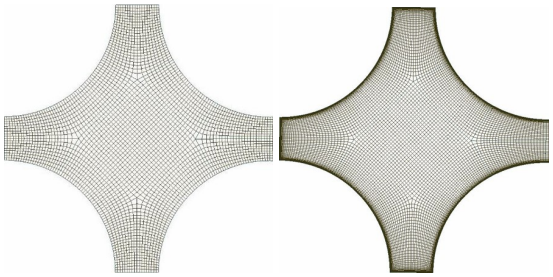

Figure 2. Meshes produced for high-*Re* (top) and low-*Re* (bottom) near-wall modelling approaches employed.

equations analytically. For example, the momentum equation is written as

$$\frac{\partial}{\partial y}\left[(\mu+\mu_t)\frac{\partial U}{\partial y}\right] = -\frac{\partial P}{\partial x} + C_u + F_u \qquad (1)$$

where C_u represents the convection terms and F_u any other forcing. By prescribing the variation of the turbulent viscosity across the near-wall cell, and with suitable approximations of the terms on the RHS, Equation 1 can be integrated analytically to give an expression for $U(y)$. This can then be used to estimate the wall-shear stress, and other quantities such as cell-averaged turbulent production, as is done in the SWF approach. The AWF approach has demonstrated considerable success in a range of flows, including mixed convection flow in a vertical pipe and a two-dimensional wall jet (Craft *et al.*, 2002, 2006).

Two types of mesh were produced to reflect the needs of the two near-wall approaches discussed above. For the wall-function approaches, the first node is positioned such that the non-dimensional distance from the wall $y^+ \approx 30$, whilst for the low-*Re* approach this is reduced to $y^+ \approx 1$. After grid refinement tests, the meshes adopted used 104256 cells for the low-*Re* approaches and 36880 cells for the wall functions. Both meshes use block-structured hexahedral elements with smoothing applied to improve orthogonality, and typical examples are shown in Figure 2.

Solver

The above turbulence and near-wall modelling approaches have been implemented into an extended version of the STREAM code (Lien & Leschziner, 1994*a*), which is a fully elliptic 3D finite volume solver capable of handling multi-block structured non-orthogonal meshes. Convective terms for all transport equations have been treated with the Upstream Monotonic Interpolation for Scalar Transport (UMIST) scheme of Lien & Leschziner (1994*b*), which is a bounded, monotonic implementation of the quadratic QUICK interpolation scheme. The code uses the standardized Message Passing Interface (MPI) for parallelisation.

RESULTS

Wall Shear Stress

Figure 3 compares predictions of the wall shear stress along the top rod surface for all model combinations tested against the experimental data of Hooper. Most models tested demonstrate good qualitative agreement with the experimental data, correctly reproducing the characteristic

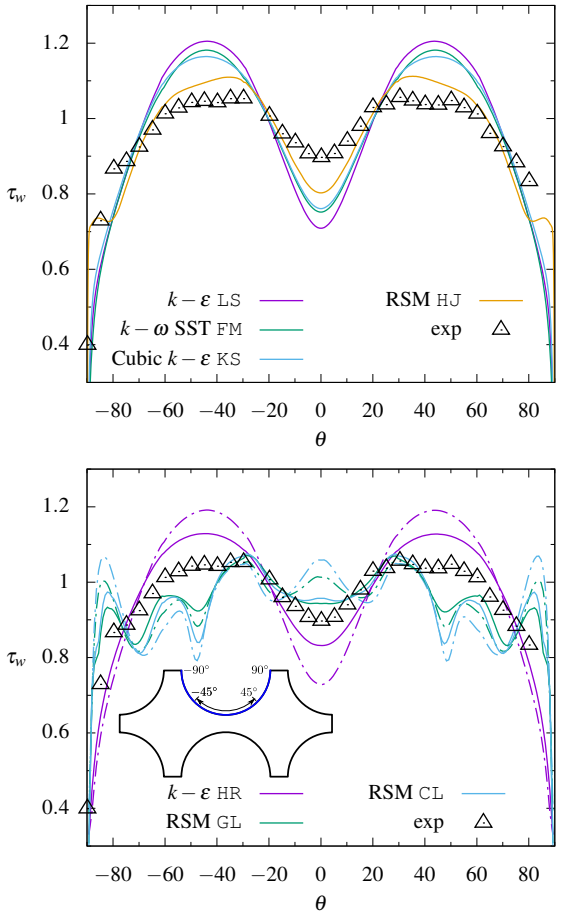

Figure 3. Wall shear stress along the top central rod (as inset bottom) for (top) low-*Re* and (bottom) high-*Re* approaches, where solid indicates AWF and dashed SWF.

'double hump'. In the low-*Re* approaches, the more advanced HJ RSM provides the best quantitative agreement, with the non-linear KS closure providing a small, but noticeable, improvement over the two linear EVMs (LS and FM). In the high-*Re* approaches, the linear EVM (HR) provides results quantitatively similar to its low-*Re* counterparts, with the more advanced analytical wall function approach offering significant improvements.

The two SWF RSMs (GL and CL), however, display more curious behaviour. Here, significant dips in τ_w are predicted at $\pm 45^\circ$ (where the perpendicular bisector of the rod wall intersects the sub-channel centre) and elevated levels of τ_w are seen at 0° within the rod gap. Whilst it is unclear whether the experiment would have the resolution to capture such an effect if it did exist, the behaviour can potentially be linked to the failure of the SWF approach in coping with the additional (correct) secondary motion that the RSMs can capture. This is discussed in more detail later, but at $\pm 45^\circ$ the secondary motion (which lies in the cross-sectional plane) is directed away from the walls and at 0° the motion is directed towards the walls. In such a flow, the wall parallel (axial) velocity is unlikely to satisfy a log-law since the convection effects implied by the secondary flows are not accounted for in the log-law formulation (convection effects are in fact specifically ignored). The analytical wall function does include such effects and it is therefore not surprising that it produces better quantitative behaviour. For the HR model the AWF brings both the peaks and dips

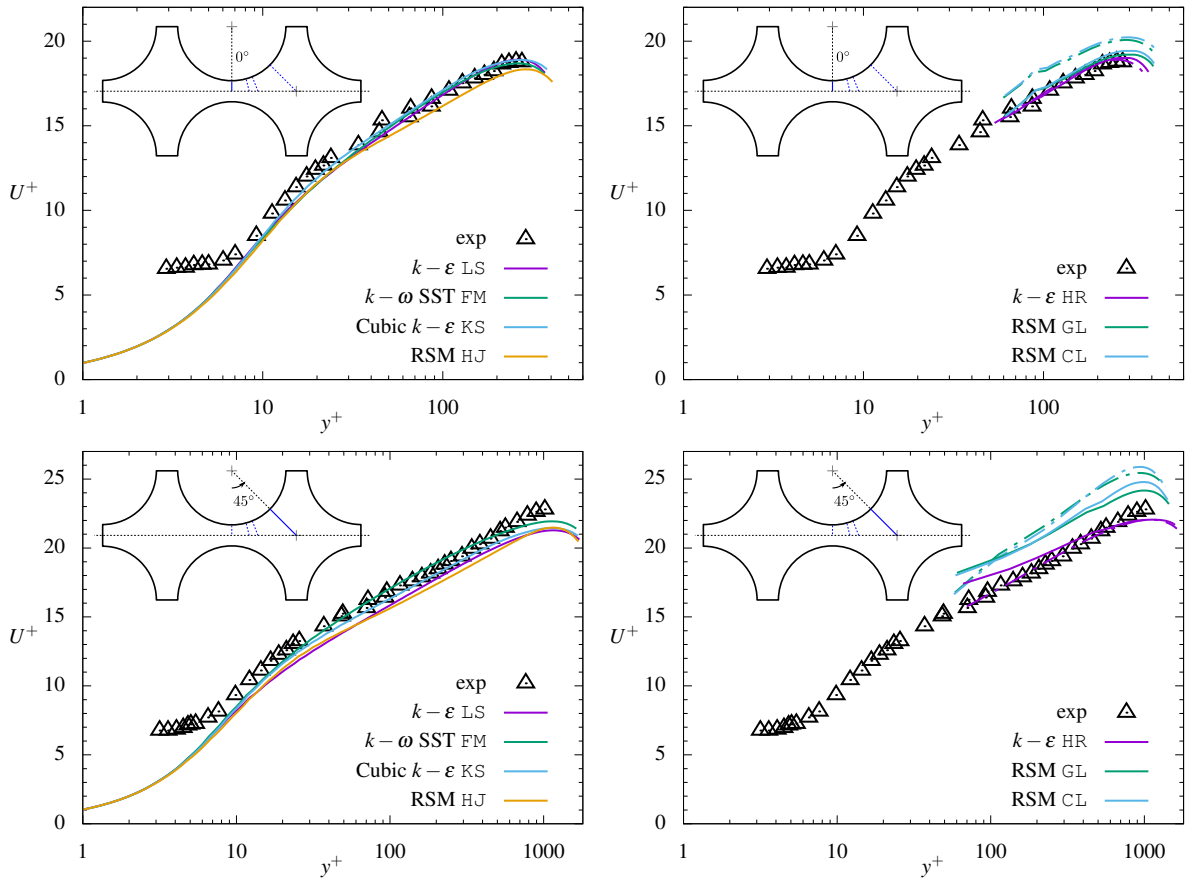

Figure 4. Velocity profiles along the gap centre (top) and at $\pm 45^\circ$ away from the centre of the top rod (bottom), indicated inset, for low-*Re* models (left) and high-*Re* models (right), where solid lines indicates AWF and dashed lines SWF.

closer to the experimental data, and for the two SWF RSMs, it nearly eliminates the discrepancy in τ_w that can be found at 0°.

Velocity and Turbulent Shear Stress Profiles

Velocity profiles along the gap centre and at $\pm 45^\circ$ away from the centre of the top middle rod are shown in Figure 4 for all models considered. In the gap centre agreement between the experimental data and the low-*Re* models is good, with the profile predicted by the HJ model slightly below the experimental data. This slight under prediction is also seen for the other low-*Re* models in the profile taken at $\pm 45^\circ$, with exception of the $k-\omega$ SST (FM) which lies slightly above. Both of these differences are likely to be within the experimental error associated with the experimental points, but unfortunately this was not quantified by Hooper in the paper.

For the high-*Re* models on the right hand side of Figure 4, the standard wall-function approach can be seen to over predict both profiles (0° and $\pm 45^\circ$) when used with the two RSMs. In both cases the AWF offers improvements, achieving excellent agreement for the profile at 0°. At $\pm 45^\circ$ some of the over prediction with the RSMs could be attributed to the under prediction in τ_w in this region, since U^+ is scaled by the friction velocity (and thus essentially $\sqrt{\tau_w}$), but this is not entirely consistent with the predictions shown along 0° line (where an over prediction of τ_w did not lead to an under prediction in U^+). However, since a) a comparison between the low-*Re* RSM and EVM approaches (on the left of Figure 4) indicates that the effects of the secondary motion on the axial velocity profile are generally small and b) the high-*Re* EVM approach gave generally good agreement, the discrepancies shown by the high-*Re* RSMs can probably be attributed towards interactions between the secondary motion (however small) and the wall-function formulation.

Figure 5 presents predictions of the turbulent shear stress ($\overline{uv}$) along the gap centre and at $\pm 45^\circ$ away from the centre of the top middle rod. The low-*Re* models again provide excellent agreement along the gap centre (0°) with some slight deviations in shape shown for the profile at $\pm 45^\circ$. Here, all models deviate below the experimental data just after the near-wall peak. The HJ RSM is the least affected and provides the best quantitative agreement. The other models all under predict the gradient of $\overline{uv}$, leading to an over prediction towards the subchannel centre.

With the wall-function approach there is clearly less consistency between the various models employed. Along the rod gap (0°) the AWF again offers improvements for both RSMs tested but slightly reduces agreement for the HR $k-\varepsilon$. The discrepancies at the start of the profiles (close to the wall) are most likely due to large changes in the wall-normal cell size, which result from the mesh requirements imposed by the wall-function approach. At $\pm 45^\circ$, and excluding the near-wall cell value, the RSMs provide generally good agreement with the experimental data with little difference seen between the AWF and SWF approach. The HR EVM shows more erratic behaviour, initially producing a significant under prediction before recovering to provide an over prediction towards the sub-channel centre.

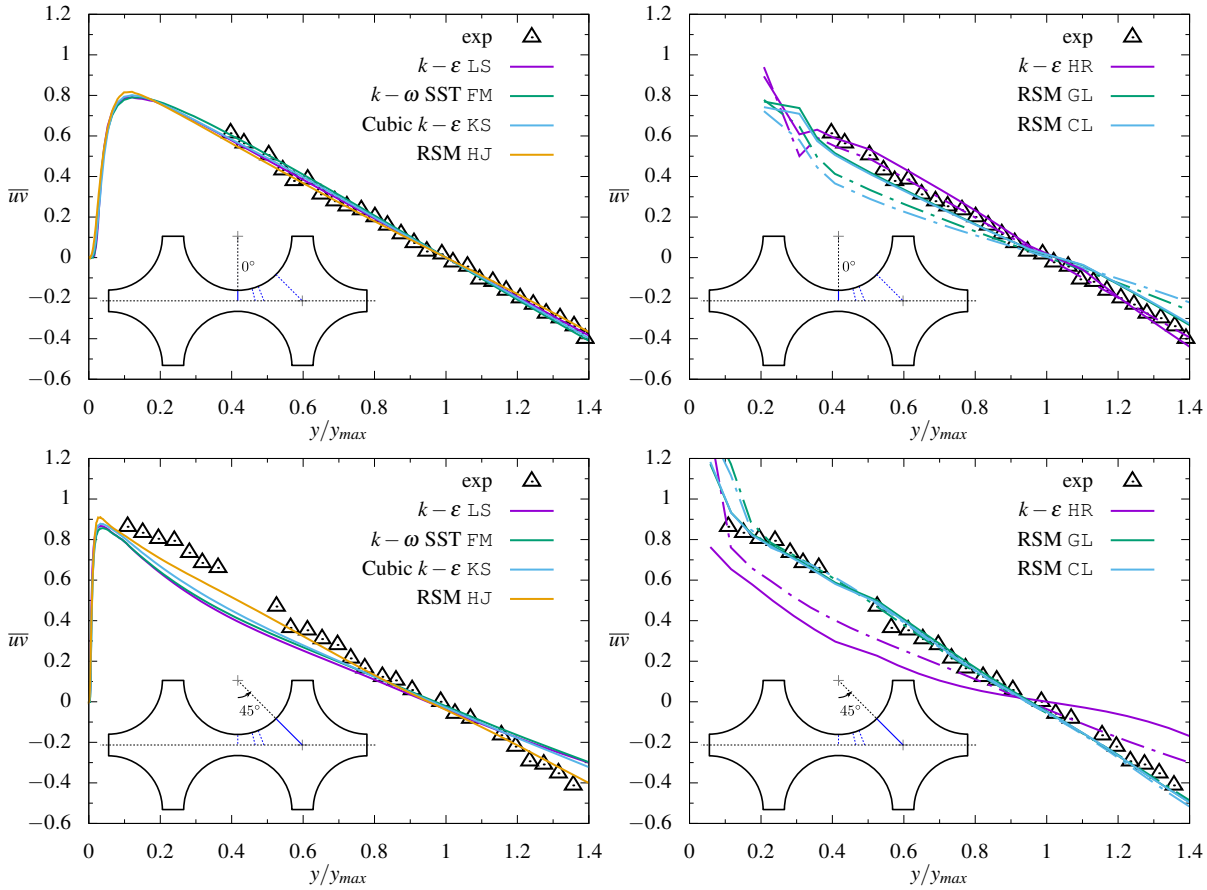

Figure 5. Turbulent shear stress ($\overline{uv}$) profiles along the gap centre (top) and at $\pm 45°$ away from the centre of the top rod (bottom), indicated inset, for low-*Re* models (left) and high-*Re* models (right), where solid indicates AWF and dashed SWF.

Secondary Motion

As discussed in the introduction, secondary motion is driven by anisotropy in the Reynolds stresses and thus only those models capable of reproducing stress anisotropy are expected to be able to correctly model it. Figure 6 visualises the secondary motion predicted by the KS Cubic NLEVM (top half) and the HJ RSM (bottom half) by superimposing streamlines over contours of the axial velocity for one of the sub-channels. The secondary motion comprises a number of counter-rotating cells, which tend to move fluid from the channel centre towards the boundaries furthest away (that is, not towards the closer rod wall). Once the flow reaches these boundaries it follows the rod surface until meeting the adjacent cell at $\pm 45°$. It then returns towards the centre of the channel completing the circulation. Some black arrows have been added to the streamlines to better illustrate the direction of the cells. The NLEVM captures the secondary cells quite well though the magnitude of the motion (0.32% of mean axial) was noticeably less than that predicted by the RSM (2.1% of mean axial). As expected, none of the linear eddy-viscosity models captured any secondary motion.

Whilst the magnitude of the secondary motion is evidently only small, it can alter the distribution of axial velocity. This is illustrated in the left of Figure 6, where contours of the axial mean velocity for a number of the models considered in this work are presented. The figure splits the left sub-channel into quadrants, where each quadrant presents the contours as predicted by the indicated model. The two EVMs (LS, FM) presented show the inner contour line, at the centre of the sub-channel, to be nearly circular. In contrast, the HJ RSM and KS cubic $k-\varepsilon$, predict this curvature to be significantly reduced. This is as a result of the secondary motion moving fluid (and thus momentum) away from the $\pm 45°$ on the rod walls and towards the centre.

CONCLUSION

CFD simulations of the flow through a square-arrayed twin-subchannel geometry typical of those found in nuclear thermal-hydraulic applications have been presented. A wide range of turbulence models (linear eddy-viscosity, non-linear eddy-viscosity and stress-transport) have been applied and the use of different near-wall treatments (low-*Re*, standard and analytical wall-functions) has also been considered. For those models which can capture turbulence anisotropy, the results revealed significant qualitative differences between the two near-wall modelling approaches applied. Both high-*Re* Reynolds stress models tested (Gibson-Launder, GL, and Craft-Launder, CL) predicted wall shear stress profiles which deviated from the experimental data at locations on the rod surface where effects from secondary motion were present. Owing to its ability to include convection and pressure-gradient effects, the more advanced analytical wall-function approach offered significantly better agreement, though did not remove the deviations entirely. All the low-*Re* models tested, including the EVMs, offered qualitatively correct results, with the full stress-transport closure of Hanjalić & Jakirlić (HJ) providing the best quantitative agreement.

Models based on the linear eddy-viscosity formulation

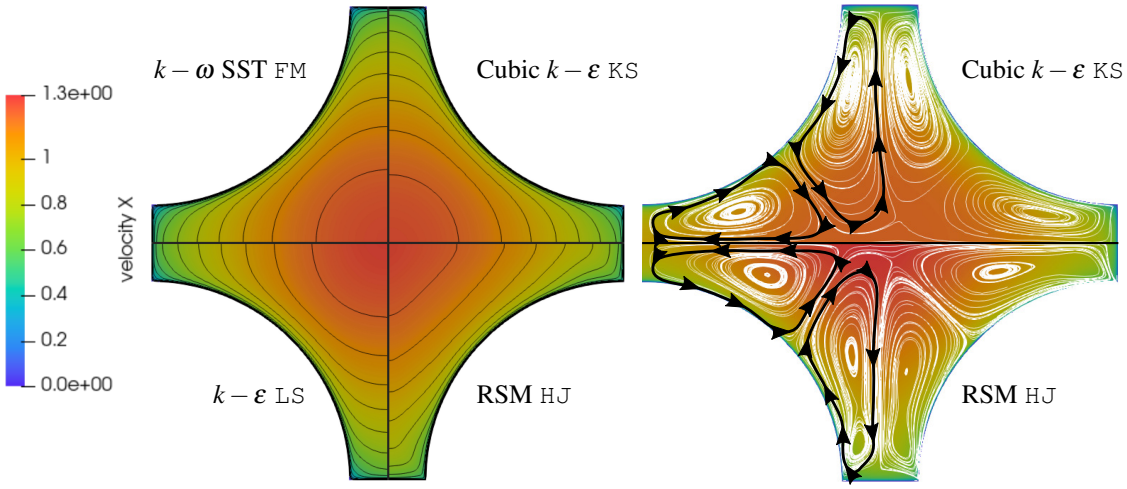

Figure 6. Left: Contours of axial velocity split into quadrants for the four models indicated. Right: as left but with KS cubic $k-\varepsilon$ model (top half) and HJ RSM (bottom half) and in-plane streamlines superimposed to illustrate the predicted secondary motion.

could not reproduce the expected secondary motion and thus failed to capture the deformation in the distribution of mean axial velocity this produces within the sub-channel cross-section. The cubic non-linear eddy-viscosity model tested (Craft-Suga, KS) did correctly reproduce the secondary circulation cells, though the magnitude of the motion was an order of magnitude less than that produced by the RSMs.

Overall, the results demonstrate both the failure of the standard wall function approach in reproducing flows with significant near-wall convection and pressure-gradient effects, and the limitations of using linear eddy-viscosity approaches in flows with significant anisotropic effects. Whilst the superiority of the low-*Re* near-wall approach is clear, the analytical wall-function tested here does demonstrate significant improvements over the standard 'log-law' based formulation and is thus recommended if computational resources do not allow a full low-*Re* approach.

REFERENCES

Craft, T., Launder, B. & Suga, K. 1996 Development and application of a cubic eddy-viscosity model of turbulence. *International Journal of Heat and Fluid Flow* **17** (2), 108–115.

Craft, T J, Gant, S E, Gerasimov, A V, Iacovides, H & Launder, B E 2006 Development and application of wall-function treatments for turbulent forced and mixed convection flows. *Fluid Dynamics Research* **38** (2-3), 127–144.

Craft, T. J., Gerasimov, A. V., Iacovides, H. & Launder, B. E. 2002 Progress in the generalization of wall-function treatments. *International Journal of Heat and Fluid Flow* **23** (2), 148–160.

Craft, T. J. & Launder, B. E. 1992 New Wall-Reflection Model Applied to the Turbulent Impinging Jet. *AIAA Journal* **30** (12), 2970–2972.

Gerasimov, A. V. 2004 Development and validation of an analytical wall-function strategy for modelling forced, mixed and natural convection flows. Ph.D., University of Manchester : UMIST.

Gibson, M. & Launder, B. E. 1978 Ground Effects on Pressure Fluctuations in the Atmospheric Boundary Layer. *Journal of Fluid Mechanics* **86** (03), 491–511.

Hanjalić, K, Jakirlić, S & Hadžić, I 1997 Expanding the limits of "equilibrium" second-moment turbulence closures. *Fluid Dynamics Research* **20** (1-6), 25–41.

Hooper, J. D. 1980 Developed single phase turbulent flow through a square-pitch rod cluster. *Nuclear Engineering and Design* **60** (3), 365–379.

Horváth, Á. & Dressel, B. 2012 Numerical simulations of square arrayed rod bundles. *Nuclear Engineering and Design* **247** (Supplement C), 168–182.

Jakirlic, S., Hanjalic, K. & Tropea, C. 2002 Modeling Rotating and Swirling Turbulent Flows: A Perpetual Challenge. *AIAA Journal* **40** (10), 1984–1996.

Jakirlić, S. & Hanjalić, K. 1995 A second-moment closure for non-equilibrium and separating high- and low-Re-number flows. In *10th Symposium on Turbulent Shear Flows*, pp. 23–30. Pennsylvania State University.

Launder, B., Reece, G. J. & Rodi, W. 1975 Progress in the development of a Reynolds-stress turbulence closure. *Journal of Fluid Mechanics* **68** (03), 537–566.

Launder, B. & Sharma, B. 1974 Application of the energy-dissipation model of turbulence to the calculation of flow near a spinning disc. *Letters in Heat and Mass Transfer* **1** (2), 131–137.

Launder, B. & Spalding, D. 1974 The numerical computation of turbulent flows. *Computer Methods in Applied Mechanics and Engineering* **3** (2), 269–289.

Lien, F. & Leschziner, M. 1994*a* A general non-orthogonal collocated finite volume algorithm for turbulent flow at all speeds incorporating second-moment turbulence-transport closure, Part 1: Computational implementation. *Computer Methods in Applied Mechanics and Engineering* **114** (1–2), 123–148.

Lien, F. & Leschziner, M. 1994*b* Upstream monotonic interpolation for scalar transport with application to complex turbulent flows. *International Journal for Numerical Methods in Fluids* **19** (6), 527–548.

Menter, F. R. 1994 Two-equation eddy-viscosity turbulence models for engineering applications. *AIAA Journal* **32** (8), 1598–1605.